Analyses of damaged effects on jacket type offshore platform

Authors:

Assoc.Prof. Engin Gucuyen, PhD. CE
Manisa Celal Bayar University, Turkey
Department of Civil Engineering
engin.gucuyen@cbu.edu.tr
Corresponding author

Selim Coșkun, MCE
Manisa Celal Bayar University, Turkey
Department of Civil Engineering
selim.coskun@yahoo.com

Assoc.Prof. R. Tugrul Erdem, PhD. CE
Manisa Celal Bayar University, Turkey
Department of Civil Engineering
tugrul.erdem@cbu.edu.tr

Engin Gücüyen, Selim Coșkun, R. Tuğrul Erdem

Analyses of damaged effects on jacket type offshore platform

In this paper, an offshore platform subjected to dynamic loading for different damage cases was modelled via fluid-structure interaction (FSI) analysis. Different damage models were considered in the case where one leg was broken, and the Young's modulus of the damaged member was reduced with four different severity ratios. In addition to the five damaged structures, the undamaged structure was modelled according to two different leg spacing conditions. Thus, the damaged models were compared among themselves as well as with undamaged models. In this study, models were investigated using a numerical FSI technique. The numerical technique was verified using semi-analytical modelling. At this stage, the equation of motion of one of the structural models was solved using a semi-analytical method based on a multi-degree-of-freedom system. In addition, the numerical environment model was verified using a semi-analytical solution of the free-surface motion equation and the wave velocity-wave force curve. An Abaqus finite-element analysis program was used to model the structures and their surroundings. While the structures were modelled using the Lagrangian technique, the fluid surroundings were modelled using the Eulerian technique. Both the conditions of leg spacing and different severity ratios were modelled, and the most negative damage type was revealed.

Engin Gücüyen, Selim Coșkun, R. Tuğrul Erdem

Analize učinaka oštećenja na rešetkasto postolje izvanobalne platforme

U ovom je istraživanju izvanobalna platforma, koja je podvrgnuta dinamičkom opterećenju za različite slučajeve oštećenja, modelirana analizom interakcije fluida i konstrukcije (engl. fluid-structure interaction - FSI). Razmatrani su različiti modeli oštećenja u slučaju kada je jedan stup bio oštećen, a Youngov modul oštećenog elementa smanjen je s četiri različita omjera intenziteta. Osim pet oštećenih konstrukcija, neoštećena je konstrukcija modelirana prema dva različita uvjeta razmaka stupova. Na taj su način oštećeni modeli uspoređivani i međusobno i s neoštećenim modelima. U ovom su radu modeli ispitivani primjenom numeričkog FSI postupka. Numerički postupak potvrđen je poluanalitičkim modeliranjem. U ovoj je fazi jednadžba gibanja jednog od konstrukcijskih modela riješena poluanalitičkom metodom temeljenom na sustavu s više stupnjeva slobode. Osim toga, numerički model okoline potvrđen je primjenom poluanalitičkog rješenja jednadžbe gibanja slobodne površine i krivulje valna brzina-valna sila. Za modeliranje konstrukcija i njihove okoline upotrijebljen je program Abaqus, utemeljen na metodi konačnih elemenata. Konstrukcije su modelirane primjenom Lagrangeova postupka, fluidno okruženje je modelirano primjenom Eulerova postupka. Modelirani su i uvjeti razmaka stupova i različiti omjeri intenziteta, te je zabilježen najnegativniji tip oštećenja.

1. Introduction

Currently, due to the increasing energy demand in the world, renewable and exhaustible resources must be offered for consumption. Offshore energy platforms comprise a platform under the facility and a substructure that carries the platform and its foundation. Jacket-type structures are more widely used as substructures than monopiles, multipiles, and gravity-based structures [1, 2].

The construction of offshore structures is more difficult for those on land, and adverse environmental situations, including wave-wind conditions and difficulties in assembling and disassembling, are unfavourable scenarios that may occur and should be considered during the construction phase. These negative scenarios can be listed as the situations that may cause damage including fatigue, corrosion, vessel impact, dropped object, design-fabrication-installation faults, and ice damage [3, 4]. Studies on damage situations can be divided into two categories based on literature surveys. The first is pre-damage studies that contain damage and damage estimation, and the second is post-damage studies that investigate the behaviour of the damaged structure.

In [5], the rate of signal energy was used for the damage detection of an offshore platform. Experimentally measured accelerations were used to compute the rate of signal energy for dented members, which reduced the section properties and eliminated damage scenarios from the primary members. Sensors were located on intact or damaged structural models. Only the sensors around dented, removed, or damaged members have a desirable signal energy rate. At the end of the study, the conformity between desirable rate of signal energy in sensors and the location of damages were detected. In another study, the amount and location of the damage were experimentally and numerically investigated [6]. Three different deep learning methods were utilised for damage detection, damage localisation, and severity estimation for the simulated damage cases. Deep learning methods for damage detection have been validated through numerical applications and laboratory tests of structures. Another study [7] focused on the amount and location of the damage. In the evaluation method, damage locations were first identified. Subsequently, the severity of the damage was determined. An iterative modal strain energy method based on modal frequencies and mode shapes was adopted to locate and quantify the damage to the structure. The feasibility and effectiveness of these methods were validated using numerical models. Researchers have investigated the effect of environmental changes, such as temperature, on the damage location using the strain energy decomposition method with modal parameters, as in their previous study [8].

A postdamage study was performed in [9]. The researchers investigated the behaviour of jacket-type offshore structures damaged by corrosion under environmental loads. The undamaged state of the numerical model was also modelled under the same environmental loads. Thus, the effect of damage caused by corrosion on the structural behaviour was examined. The effects of the damage caused by corrosion on pipelines were studied in [10]. The corrosion effect was investigated by modelling the behaviour of damaged and undamaged structures under the same environmental loads using the Abaqus finite element analysis program. Another post-damage study performed by [11] investigated different repair methods for different damage cases, such as perforation, dent, failure, and strength reduction, to investigate ideal solutions for selecting alternative repair methods. In [12], the load distributions among tubular members after a collision between an offshore platform and ship were examined. Different collision velocities and locations caused different types of deterioration, such as dents and fractures.

According to a literature survey, damage scenarios can appear as member dents, reduce section properties, and remove primary members. In this study, a reduction in section properties and removal of members were utilised to model the deterioration of a four-legged jacket-type offshore platform. In addition, in the case of a four-legged model that continues to operate with three legs because of local rupture in one leg, the changes in its structural behaviour have also been investigated and compared to the those in the undamaged three-legged model.

To estimate the dynamic response of offshore structures under environmental loads, fluid-structure interaction (FSI) methods are commonly used to investigate the dynamic behaviour of structures. The FSI analyses of coupling attributes were classified as one- or two-way. Finite element analysis was applied to both analyses. An FSI analysis supported by finite elements can be performed using either the Eulerian technique [13, 14] or the Lagrangian technique [15]. In addition, both techniques can be used in arbitrary Lagrangian–Eulerian (ALE) [16, 17] and coupled Eulerian–Lagrangian (CEL) [18] analyses. The Abaqus finite element program is widely used by researchers for interaction modelling [19].

In this study, three-dimensional finite element models of the structures and surroundings were modelled within the framework (ABAQUS/CAE) via CEL, one of which was modelled as a multi-degree-of-freedom system [20]. The equation of motion of the multi-degree-of-freedom system was solved using the semi-analytical Runge-Kutta method. Thus, structural verification of the numerical model was performed. The flow environment was investigated by determining the motion of the free water surface according to CEL analysis. In addition, the wave velocities and forces were obtained from CEL analysis. This step was verified using a semi-analytical method by computing Eqs. (1) to (4).

In the damage modelling phase, five scenarios were examined. In the first four cases, damage was achieved by reducing the Young's moduli of the damaged members with different severity ratios as follows: 5 %, 10 %, 20 % and 50 %. In the fifth scenario, damage occurred owing to the removal of part of the leg member. In the comparison and contrast phases

of the study, the damaged structures were compared with intact four- and three-legged structures. A comparison was performed based on the structural behaviour of the undamaged three-legged structure and the damaged four-legged structure, one of the legs of which was ruptured or damaged at different rates.

2. Structural models and environmental conditions

In the modelling phase, seven different jacket structural models, six of which were four-legged and one was three-legged, were analysed. The four-legged structure modelled using the Lagrangian technique and the marine environment modelled using the Eulerian technique are shown in Figure 1. B, b, and d and indicate the base, base-side length, and water depth, respectively.
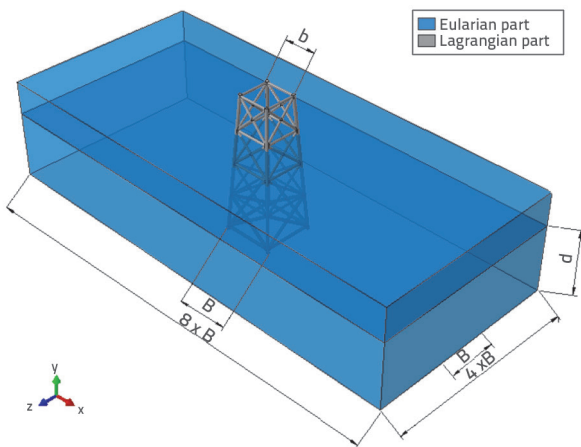
Figure 1. Coupled model and dimensions

The numerical and simplified semi-analytical structural models are shown in Figure 2, where h is the floor height, F is the external force affecting the stories, m is the floor mass, and k is the floor stiffness. Wave and wind loads were defined as environmental conditions in the numerical analyses.
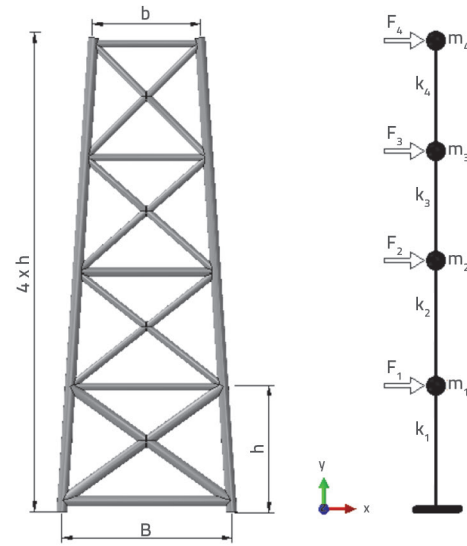
Figure 2. Numerical and semi-analytical models

2.1. Structural models

Jackets typically consist of corner legs fixed to the seabed and interconnected by horizontal and diagonal bracing. The Base dimensions of the four-legged structural model (× BxB) were 22 m × 22 m, as shown in Figure 1. The top dimensions were 14 m × 14 m. An equilateral triangle emerged in the three-legged structure, the base and top parts of which had the same side lengths as those in the four-legged model. The structures were modelled using a structural steel material with a Young's modulus of 210 GPa. This value was reduced at the given rates for Cases III, IV, and VI. Figure 3 shows the cases considered in this study. Although the location of the damage did not change in the damaged cases, different damage situations are represented by different colours. Seven cases are shown in the
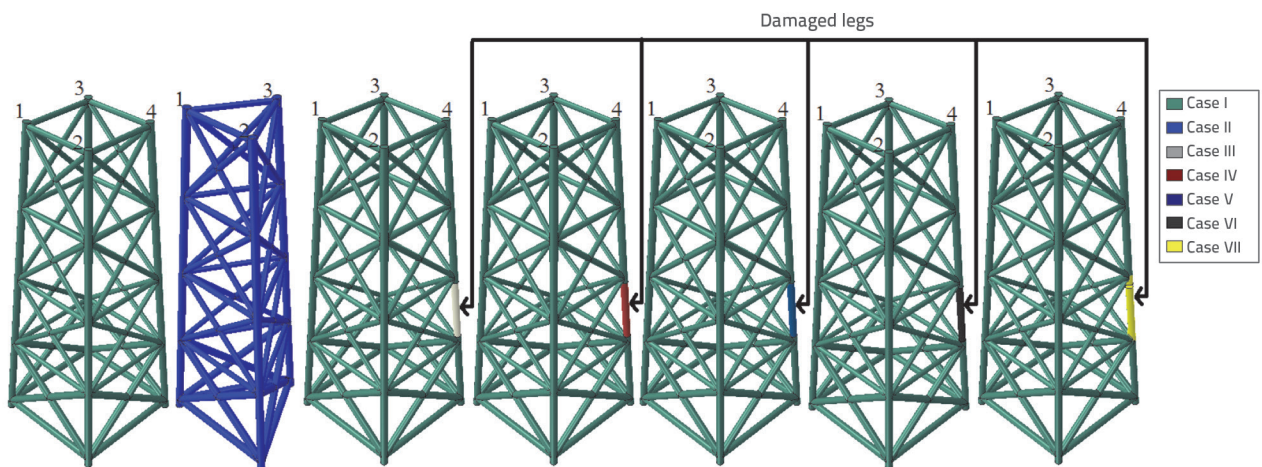
Figure 3. Structural models and cases

Table 1. Description of the cases

Condition	Case I	Case II	Case III	Case IV	Case V	Case VI	Case VII
Description	Intact four legged	Intact three legged	Damaged severity ratio 5 %	Damaged severity ratio 10 %	Damaged severity ratio 20 %	Damaged severity ratio 50 %	Damaged ruptured

figure from left to right: four intact legs, three intact legs, one leg damaged with a 5 % severity ratio, one leg damaged with a 10 % severity ratio, one leg damaged with a 20 % severity ratio, one leg damaged with a 50 % severity ratio, and one leg damaged with a ruptured member. Leg enumerations are shown in the same figure.

The Poisson's ratio was assumed to be 0.3, and the density was 7850 kg/m³. The legs of the jackets are 1.20 m in diameter and 0.012 m in thickness, and the rest of the members have the same geometrical properties with a 1.00 m diameter and 0.010 m thickness for all cases.

The structures are composed of four stories, with each story having a height (h) of 15 m. Therefore, the total height of the structures is 60 m. In contrast, the total mass of the platform is 1.50×10^5 kg. Nonstructural masses are defined as concentrated masses symmetrically located at the four corner nodes. The classification of cases according to the structural models is presented in Table 1.

2.2. Environmental conditions

The evaluated structures were considered as a combination of dead, wind, and wave loads. The first two stories of the structure, with a height of 30 m, were in contact with the water. However, the rest of the stories have a height of 30 m and are in contact with air. Wave forces affect the structural members in contact with the marine environment. The other members in contact with the air were affected by wind forces. These forces were considered in both the FSI and semi-analytic analyses.

Hydrodynamic wave forces acting on the structures were calculated with water particle velocities (u) and accelerations (ù) in accordance with the wave theory determined by the water depth where the structure deploys (d), the wave height (H), and the period (T) [21]. In this study, wave forces were calculated according to d = 30 m, T = 8 s, and H = 2 m. By adopting these values, the marine environment was modelled using the Airy (linear) wave theory. The wavelength (L_W) was calculated as 98.71 m by considering the wave parameters. Although only the wave velocity (Eq.1) was used as the input velocity in the numerical analysis, both the velocity and acceleration in Eqs. (1) and (2) were used to determine the wave forces in this semi-analytical study.

$$u = \frac{H}{2} \frac{gT}{L_W} \frac{\cosh[2\pi(y+d)/L_W]}{\cosh(2\pi d / L_W)} \cos(\frac{2\pi}{L_W} x - \frac{2\pi}{T} t) \quad (1)$$

$$\dot{u} = \frac{g\pi H}{L_W} \frac{\cosh(2\pi(y+d)/L_w)}{\cosh(2\pi d / L_w)} \sin(\frac{2\pi}{L_w} x - \frac{2\pi}{T} t) \quad (2)$$

The total horizontal force (F_H) is the sum of the wave drag force (F_D) and inertial force (F_I). The total force was obtained after integrating the forces along the length of the tower in contact with the water, as given in Eq. (3).

$$F_H = F_D + F_I = \int_{-d}^{\eta} \frac{1}{2} \rho_w C_D D u_{(y,t)} |u_{(y,t)}| dy + \int_{-d}^{\eta} \rho_w C_M \frac{\pi D^2}{4} \dot{u}_{(y,t)} dy \quad (3)$$

In Eq. (3), C_D = 0.7 and C_I = 2.0 are the drag and inertia coefficients, respectively. r_w is the saltwater density, D is the tower diameter, h is the water surface elevation, t is the time, and y is the vertical location. The surface elevation equation is as follows:

$$\eta = \frac{H}{2} \frac{gT}{L} \frac{\cosh[2\pi(y+d)/L]}{\cosh(2\pi d / L)} \quad (4)$$

In addition, the wind force which is another environmental load affecting the structure, was determined using Eq. (5), according to the Eurocode velocity profile (u_a) at any elevation above the water surface (y). Wind force (Fa) was calculated according to wind velocity (u_a).

$$u_a = U_{BAS} k_T \ln(y/z_0) \quad (5)$$

where U_{BAS} is the reference wind velocity (24 m/s), k_T is the terrain factor (0.17), and z_0 is the roughness length (0.01).

$$F_a = \int_{\eta}^{L-\eta} \frac{1}{2} \rho_a u^2_{a(y)} C_s A_{(y)} dy \quad (6)$$

In Eq. (6), A is the cross-sectional area of the member, ρ_a is the mass density of air, and C_s is the shape coefficient of the member, which was taken as 0.50 for the cylindrical sections [22].

3. Numerical study

3.1. Definition of CEL analysis

The mathematical definition of the CEL technique used by the Abaqus finite elements program is described by the following equations (7) to (9) are the mass, momentum, and Lagrangian energy conservation equations, respectively.

$$\frac{D\rho}{Dt} + \rho \nabla \cdot v = 0 \quad (7)$$

$$\rho \frac{Dv}{Dt} = \nabla \cdot \sigma + \rho b \quad (8)$$

$$\frac{De}{Dt} = \sigma : D \tag{9}$$

In Eqs. (7) to (9), material velocity, density, the Cauchy stress, the body force, and the internal energy per unit volume are represented by v, r, σ, b, and e, respectively.

$$\frac{D\varphi}{Dt} = \frac{\partial\varphi}{\partial t} + v \cdot (\nabla\varphi) \tag{10}$$

By using Eq. (10), the governing equations for the Lagrangian technique are determined in the general conservation form for the Eulerian procedure, as follows:

$$\frac{\partial\varphi}{\partial t} + \nabla \cdot \Phi = S \tag{11}$$

where j is an arbitrary solution variable, Φ is the flux function, and S is the source term in Eq. (11). This equation can be written in two different forms as follows:

$$\frac{\partial\varphi}{\partial t} = S \tag{12}$$

$$\frac{\partial\varphi}{\partial t} + \nabla \cdot \Phi = 0 \tag{13}$$

Eq. (13) is therefore the same as the standard Lagrangian formulation when the spatial time derivative is changed by the material time derivative on the fixed mesh. The deformed mesh is then transferred to the original fixed mesh. Subsequently, the volume of material transferred between adjacent elements is computed to solve Eq. (13). The variables of the Lagrangian formulation, momentum, mass, stress, and energy were then arranged to provide an account of the material flow between adjacent elements according to the transport algorithms.

3.2. Creating models by CEL analysis

The intact and empty parts were used to model the marine environment according to the Eulerian technique. The structures were modelled using the Lagrangian technique, and bidirectional FSI solutions were obtained through CEL analysis. The finite element model of Case II used in the CEL analysis is shown in Fig. 4. The bottom of the Eulerian part is a vacancy above the seawater that allows for free surface motion. Seawater is defined by the EOS material, and the material properties considered are as follows: velocity of sound (c_0) in salty water: 1560 m/s, density (μ): 1025 kg/m³, and dynamic viscosity (μ): 0.0015 Ns/m². The characteristics of the steel material assigned to the Lagrangian part are described in Section 2.1.
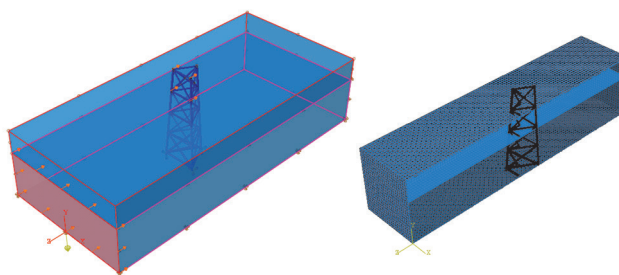
Figure 4. Boundary conditions
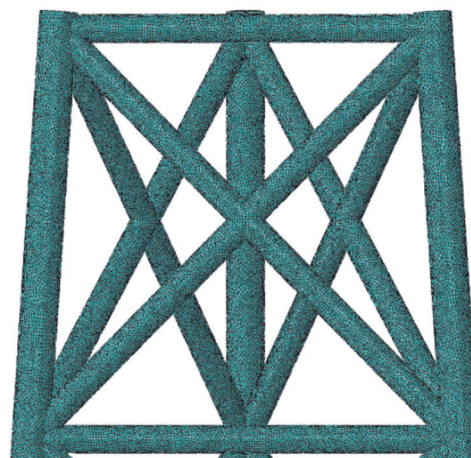
Figure 5. Mesh configuration

In Figure 4, the bottom of the Eulerian part is defined as the impermeable wall, the surfaces on the long side are defined as the far field, and the surfaces on the short side are defined as the inlet and outlet. Eq. (1) was used as the inlet velocity. Therefore, the same parameters as those of the inlet surface were implemented in the far fields. The mesh configuration of the finite elements model is shown in Figure 5. A 4-node doubly curved thin or thick shell, reduced integration, hourglass control, and finite membrane strains elements (S4R) are utilized for the Lagrangian part. Additionally, an 8-node linear Eulerian brick with reduced integration and hourglass control elements (EC3D8R) was used as the Eulerian part. Distances between the nodes were 0.01 m and 0.50 m for the Lagrangian and Eulerian parts, respectively. Thus, 19723374 nodes and 19905048 elements, 19532252 nodes and 19707492 elements, and 16857356 nodes and 16991833 elements were created for Cases I, II, and VII, respectively.

The equation of motion for the structure considered in the finite element program under external forces (F) can be written as follows:

$$m^{NJ}X^N|_t = (F^J - I^J)|_t \tag{14}$$

In Eq. (14), m^{NJ} represents the mass matrix, F^J is the externally applied load vector transferred from the Eulerian part, and I^J symbolises the internal force vector caused by the internal stresses of the elements and is the acceleration. I^J is determined

from single elements such that a global stiffness matrix does not need to be constituted. Coupled Eulerian-Lagrangian analyses can be generated in dynamic, explicit steps only via the explicit integration rule given by [19].

4. Semi analytical study

In this part of the study, numerical and semi-analytical analyses were performed simultaneously. The displacements and natural frequencies determined from the numerical analysis were verified by a semi-analytical analysis for Case I. As shown in Figure 2, the structure was idealised as a lumped-mass tower. The differential equation governing the response of a multi degree-of-freedom system is expressed by Eq. (15).

$$mX + kX = F \tag{15}$$

The displacement and natural frequency values with four degrees of freedom were determined using Eq. (15). The coordinate transformation was implemented to determine Eq. (15) from Eqs. (16) and (17). The modal shape matrix [f], which was obtained by considering the structural modes, was used for coordinate transformation.

$$\{X\} = [f]\{x\} \tag{16}$$

$$[f]^T[m][f]\{x\} + [f]^T[k][f]\{x\} = [f]^T \tag{17}$$

The matrices of mass (m) and stiffness (k) are given by Eqs. (18) and (19).

$$m = \begin{bmatrix} 2.06 \cdot 10^5 & 0 & 0 & 0 \\ 0 & 1.55 \cdot 10^5 & 0 & 0 \\ 0 & 0 & 1.47 \cdot 10^5 & 0 \\ 0 & 0 & 0 & 1.53 \cdot 10^5 \end{bmatrix} \tag{18}$$

$$k = \begin{bmatrix} 6.56 \cdot 10^5 & -2.49 \cdot 10^5 & 0 & 0 \\ -2.49 \cdot 10^5 & -4.49 \cdot 10^5 & -2.00 \cdot 10^5 & 0 \\ 0 & -2.00 \cdot 10^5 & 3.74 \cdot 10^5 & -1.74 \cdot 10^5 \\ 0 & 0 & -1.74 \cdot 10^5 & 1.74 \cdot 10^5 \end{bmatrix} \tag{19}$$

While the total wave force on the first story, $(F_{1(t)})$, was applied to node 1, the total wave force on the second story, $(F_{2(t)})$, was applied to node 2. The wind force that affects the members on the third and fourth stories was positioned at related points, similar to the wave force. The legs, horizontal bracings and wave forces affecting the diagonals in the first two stories of the model were calculated one by one according to Eq. (3). These forces were added to the story. The wind forces affecting the model were calculated using Eqs. (6) for each member in all the stories. The wind forces in the stories were determined to

be F_3=164800 N and F_4=197537 N. The wind and wave forces comprise the external forces on the right side of Eq. (15). In addition, Eq. (17) is solved using the initial conditions below via the Runge–Kutta method to achieve the point displacements.

$$\xi_{1(0)} = \xi_{2(0)} = 0, \ \dot{\xi}_{1(0)} = \dot{\xi}_{2(0)} = 0 \tag{20}$$

The Runge–Kutta method evaluates the simple relationships at the beginning, middle, and end of all overall time steps (Δt) as shown below [23].

$$\ddot{X}_{(t)} = m^{-1}\left(F_{(t)} - kX_{(t)}\right) \quad \dot{X}_{t+\Delta t} = \dot{X}_t + \ddot{X}_t\Delta t \quad X_{t+\Delta t} = X_t + \dot{X}_t\Delta t \tag{21}$$

In addition to the displacement values, the natural frequency of the structure (ω) was determined using Eq. (22).

$$[k] - w^2[m] = 0 \tag{22}$$

Both the semi-analytic and finite element methods (FEM) were continued for 64 s with a step interval (Δt) 0.01 s.

5. Results

In this section, the numerical and semi-analytical outputs of the structure and the marine environment are compared. Thus, the numerical models were verified. Subsequently, the outputs of each case were presented, and the damage effects on the structures were investigated. The wave velocities, forces, and free-surface elevations at specified points were determined using Eqs. (1), (3), and (4) and compared with the numerical model.
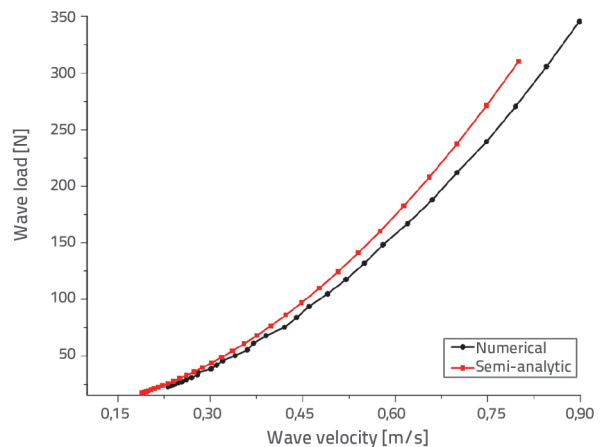
Figure 6. Variation of wave force with wave velocity

The elevation for the z = 40 m position analytically varied between -0.99 m and +0.99 m, and the elevation for the same position numerically changes between -0.90 m and +1.08 m. While the maximum horizontal wave velocity of the specified was is determined as 0.89 m/s by Eq. (1), this value was numerically computed as 0.80 m/s. The maximum horizontal wave forces were calculated as 345.65 N and 310.22 N according to Eq. (3) and the numerical analysis, respectively.

Table 2. Natural frequency and displacement values

Analysis	Natural frequency [rad/s]				Maximum displacement [m]			
	ω_1	ω_2	ω_3	ω_4	X_1	X_2	X_3	X_4
Numerical	2,759	2,769	2,775	6,262	0,103	0,252	0,421	0,611
Semi-analytical	2,979	3,031	3,055	6,922	0,112	0,276	0,468	0,688
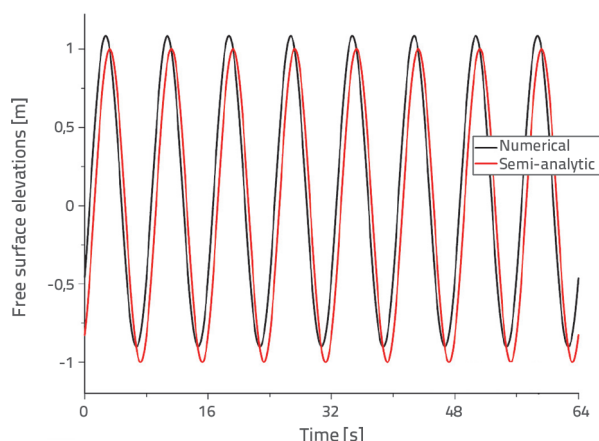
Figure 7. Wave elevations

The first four natural frequencies and displacement values of the four stories obtained by the numerical and semi-analytical modelling of the structure belonging to Case I are listed in Table 2.

The time-varying displacement values of the fourth story listed in Table 2 are shown in Figure 8. Thus, the harmony between the environmental and structural outputs was determined using semi-analytical and numerical analyses.

The displacement oscillates between a minimum 0.270 m and a maximum 0.611 m for the numerical analysis, and a minimum 0.238 m and a maximum 0.688 m for semi-analytic analysis. The mean values were 0.440 and 0.485 for the numerical and semi-analytic analyses, respectively. Subsequently, the numerical models were compared. For this purpose, the mode shapes and corresponding natural frequency values of the structure in different cases were obtained via numerical analysis using the Lanczos Method [18]. The results are presented in Figure 9.

While the maximum natural frequency value was obtained in Case I for the undamaged structure, the minimum value was determined in Case VII. When the natural frequencies of the four-legged models were compared, there was a 3.51 % decrease between Cases I and VI, and a 26.71 % decrease between Cases I and VII. In addition, a 13.99 % decrease between Cases I and II was observed when the three-legged models were compared.
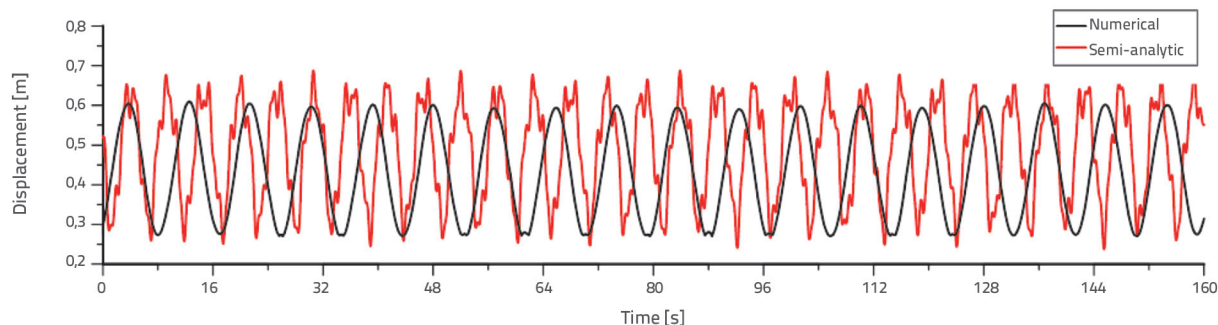
Figure 8. Time histories of motions of the structure and maximum tension of the mooring lines

$\omega_1 = 2,759$ [rad/s] $\omega_1 = 2,373$ [rad/s] $\omega_1 = 2,750$ [rad/s] $\omega_1 = 2,735$ [rad/s] $\omega_1 = 2,722$ [rad/s] $\omega_1 = 2,662$ [rad/s] $\omega_1 = 2,022$ [rad/s]
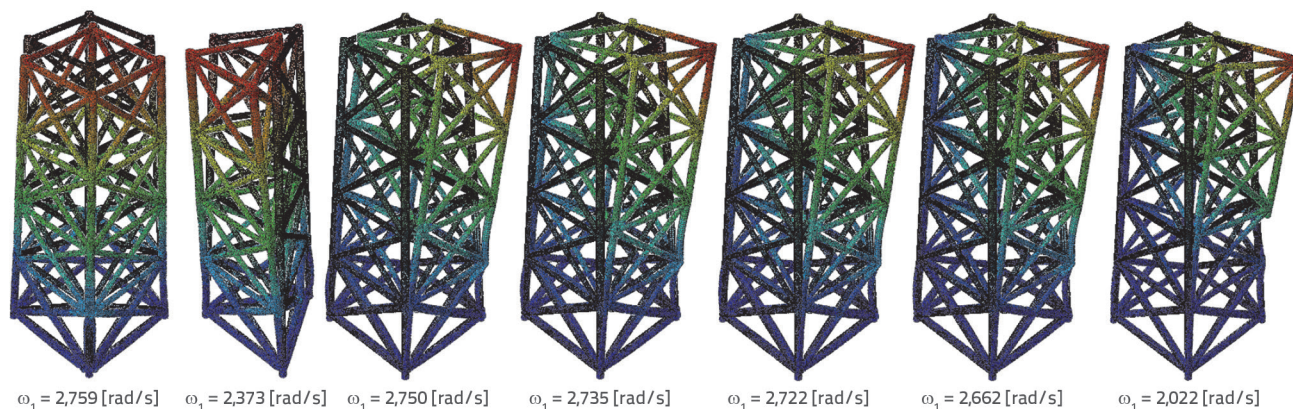
Figure 9. Mode shapes and corresponding natural frequencies of the structure

The maximum displacement and reaction force values for each leg in the investigated cases are shown in Figure 10. Whereas the third leg is presented for Case II, the change in the reaction force with displacement for the other cases in the fourth leg is shown in Figure 11.
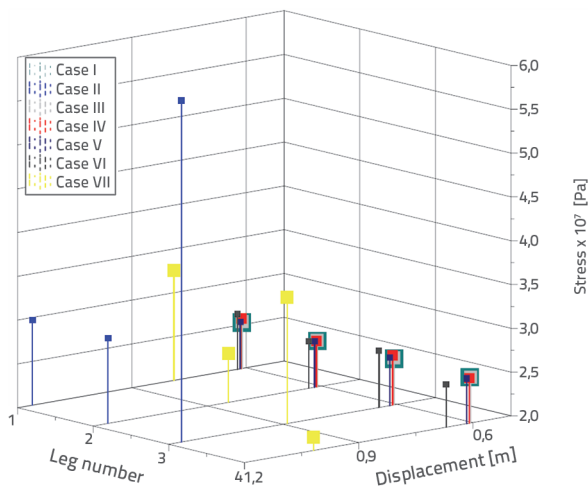
Figure 10. Stress-displacement values according to legs
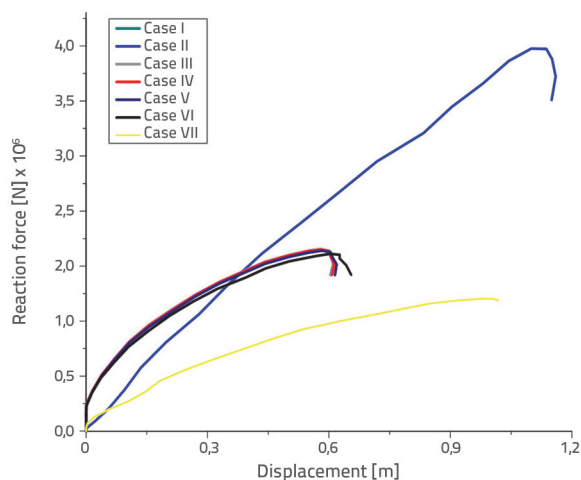
Figure 11. Reaction force-displacement curves

When the four-legged models were examined, the maximum displacement value occurred in Case VII, and the minimum value occurred in Case I. There was a 67.45 % difference between these cases. However, the minimum and maximum stress values were observed in Case VII. When Cases I and VII were compared based on the maximum stresses, a 36.45 % difference was observed between the numerical values. When the stresses in the damaged feet were investigated, a 0.18 % difference was established between Case I and Case III, a 0.31 % difference was obtained between Case I and Case IV, a 0.45 % difference was determined between Case I and Case V, 1.28 % difference was found between Case I and Case VII, and a 17.01 % difference was observed between Case I and Case VII. The maximum stress value among all models was obtained in Case II. When the reaction forces in the damaged feet were

investigated, the differences were 0.05 %, 0.20 %, 0.80 %, 2.64 %, and 37.49 % between cases I and III, cases I and IV, cases I and V, cases I and VI, and cases I and VII, respectively. Unsurprisingly, the maximum reaction force was observed in Case II.

The time-varying displacement values of the third leg for Case II and the fourth leg for the remaining cases are shown in Figure 12.
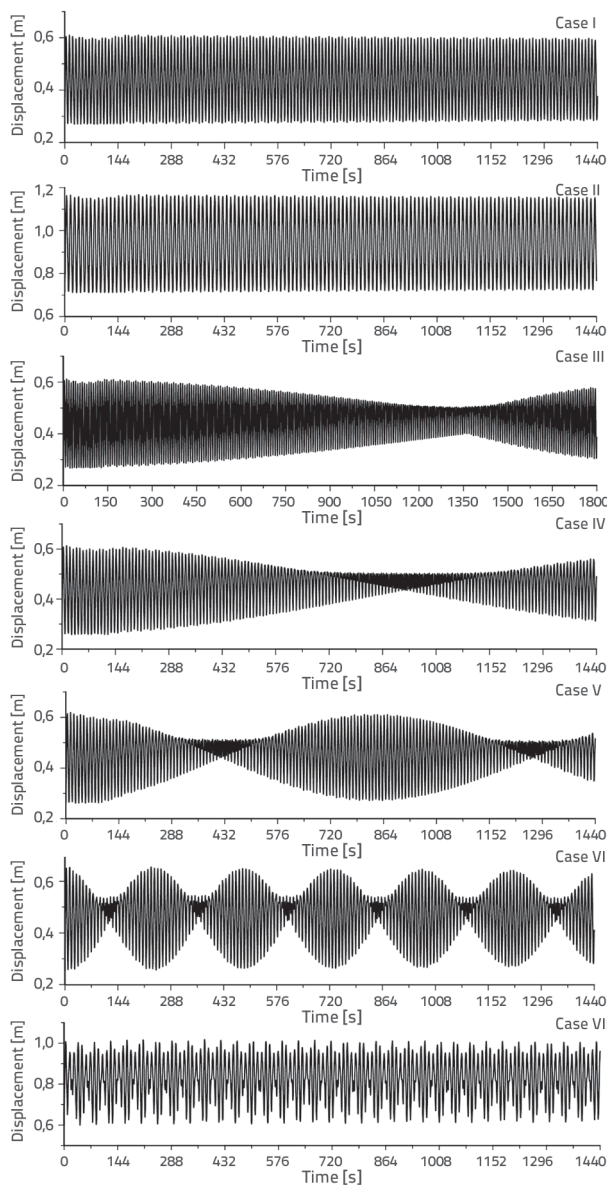
Figure 12. Time varying displacement values for each case

When the displacements of the damaged feet were examined, differences of 0.06 %, 0.18 %, 1.32 %, 10.16 % and 67.45 % were obtained between cases I and III, cases I and IV, cases I and V, cases I and VI, and cases I and VII, respectively. As expected, the maximum displacement among the damaged feet occurred in Case VII. The displacement and stress distributions for each case are presented in Figs. 13 and 14, respectively.
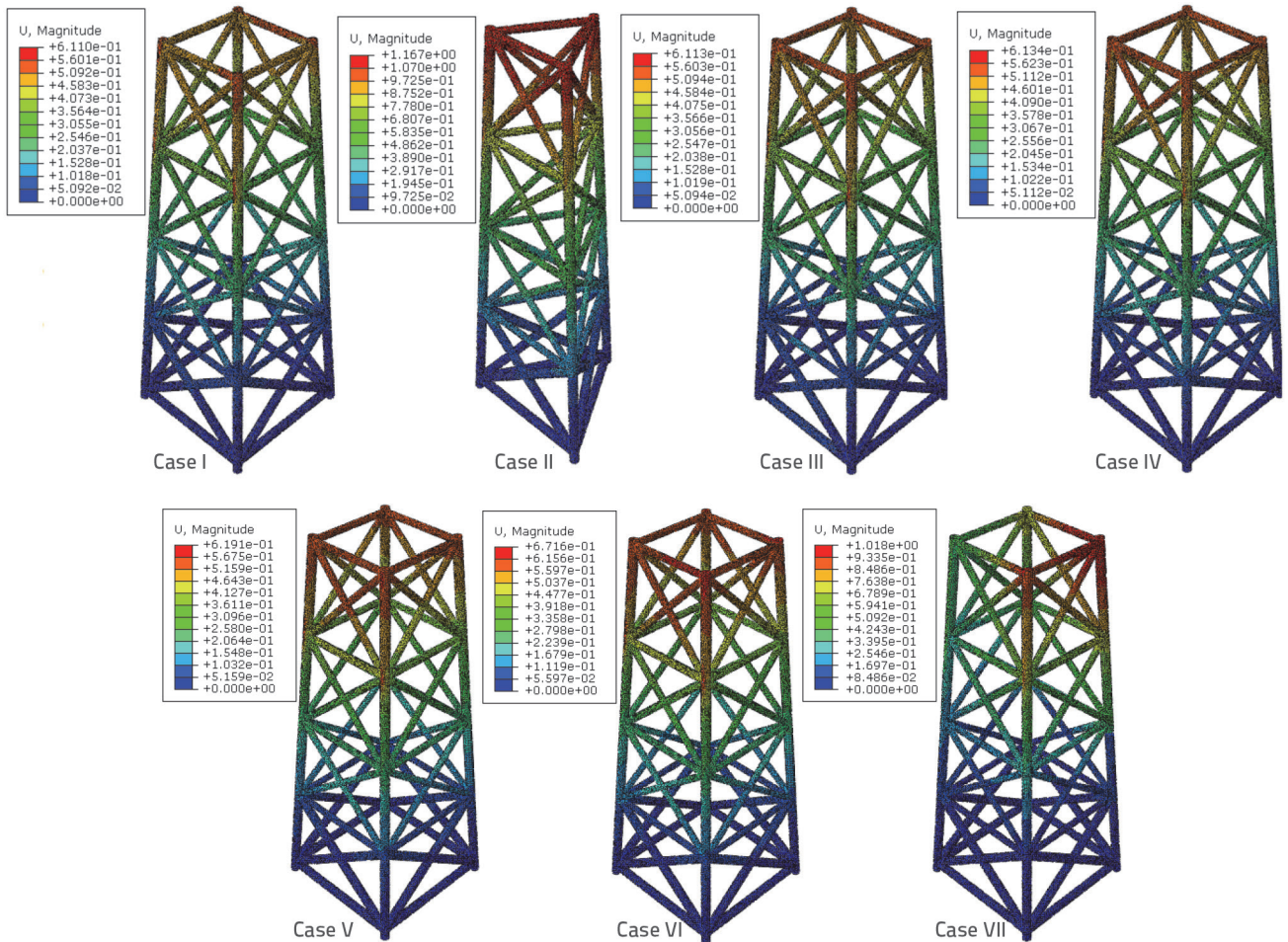
Figure 13. Displacement distributions of each case
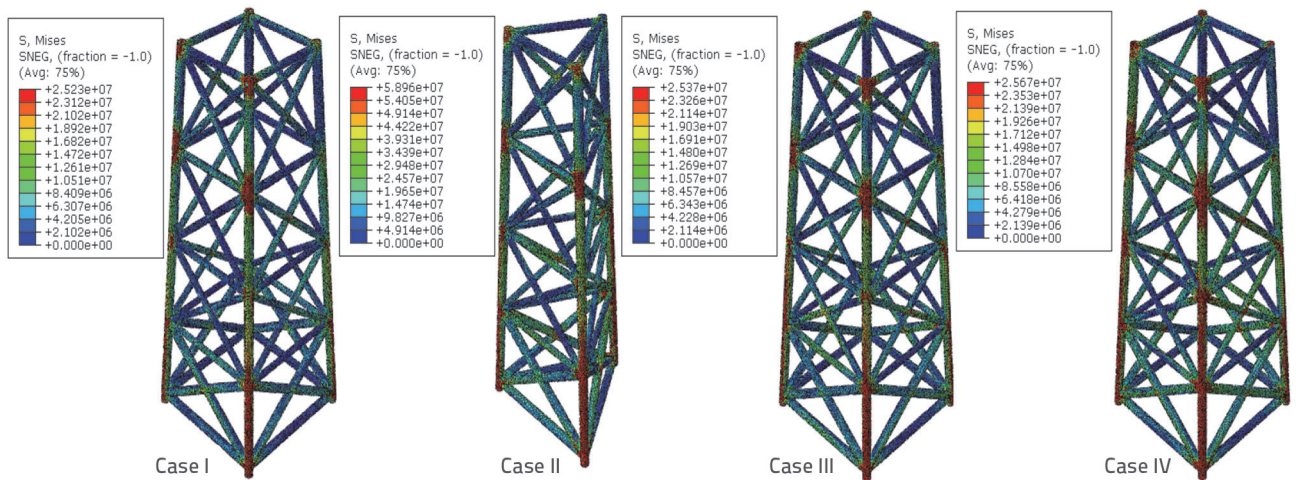
Figure 14. Stress distributions of each case, cases I to IV
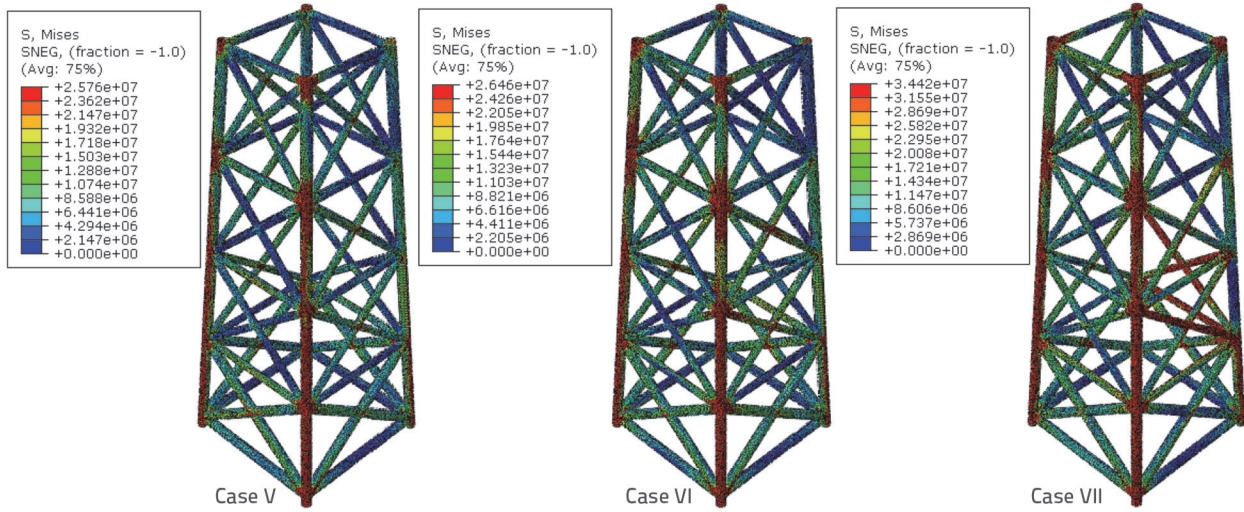
Figure 14. Stress distributions of each case, cases V to VII
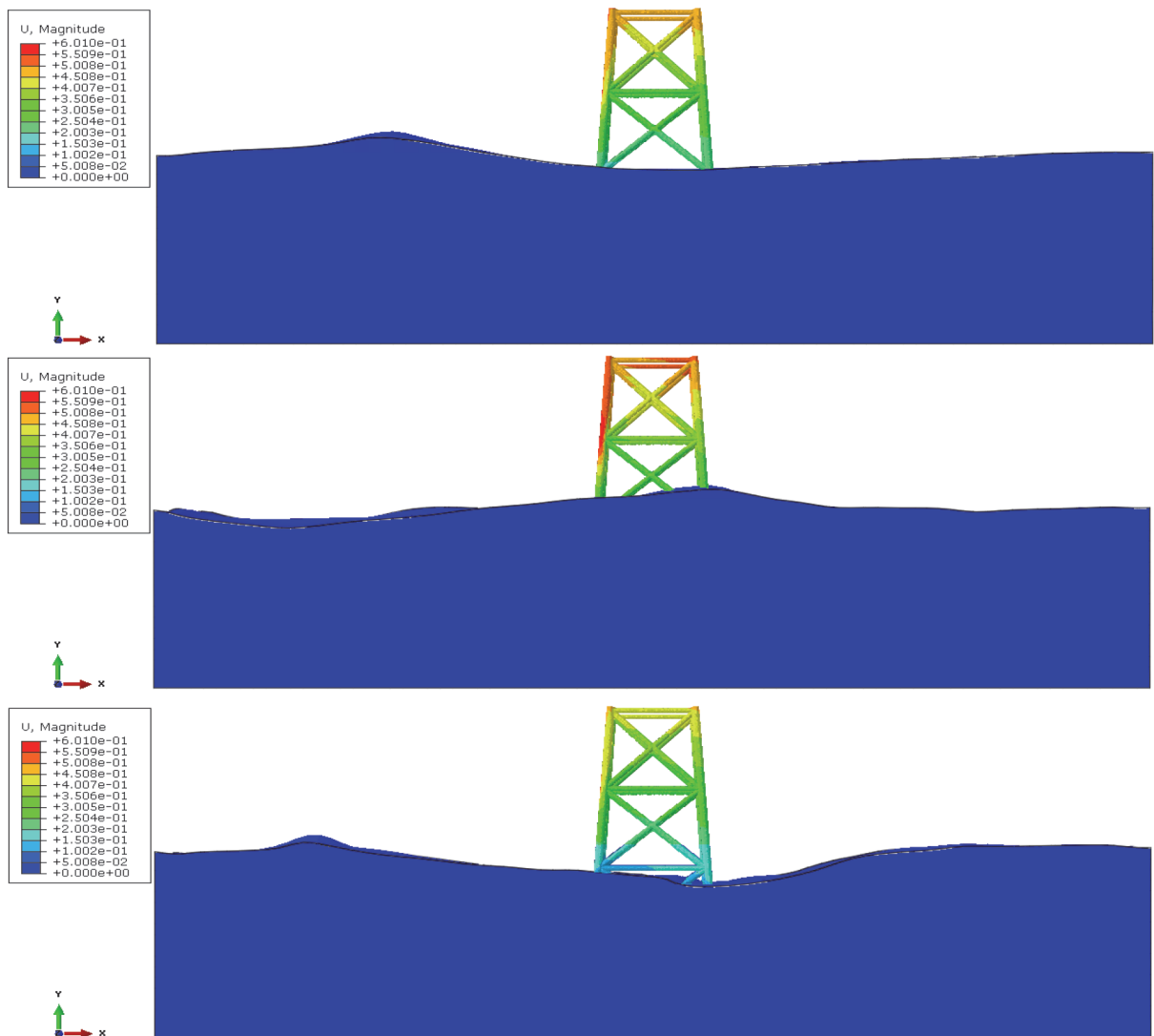
Figure 15. Coupling of Eulerian and Langrangian domains

The coupling of the Eulerian and Lagrangian parts for Case I is presented in Figure 15. The water surface movement at different moments and the displacement of the structure depending on this movement can be observed in this manner.

6. Conclusion

Truss systems which constitute the infrastructure of vital systems that operate in open seas, including energy, transportation, and defence systems, have more costly and complex structures than their equivalents on land. Consequently, sustainability is critical. To ensure sustainability, damage that may occur during construction should be considered. Therefore, five cases of the same structure with different damage types and ratios as well as an undamaged structure and another undamaged structure with different leg spacings were analysed in this study. The CEL technique was utilised in the fluid-structure interaction analyses.

First, the numerical environment and structural models were verified using semi-analytical models. While the verification of the numeric environment model is performed through surface motion and the wave velocity-wave force curve, the displacement and natural frequency values are used to verify the numerical structure model. When the accordance of free-surface elevations is analysed, only the wave model is considered without placing the structure inside. In addition, the structure of the flow deteriorates when the structure is placed inside; therefore, a comparison with the analytical method would not yield appropriate results. According to the free-surface elevations, wave velocity, and wave force, the largest differences between the analytical and numerical results were 10.50 %, 10.11 %, and 10.25 %. Therefore, the harmony of the free-surface elevations was investigated both numerically and visually.

Subsequently, the numerical structural results were verified via the solutions of the differential equations related to a multi degree-of-freedom system of Case I. The frequencies of the first four modes were determined. It can be observed from Table 2 that the difference between the two analysis types varied between 8.01 % and 10.54 %. The time-varying displacement values for the two analyses are presented in Figure 8. The maximum displacements at these points are listed in Table 2. Whereas the difference between the first-point displacements was 9.11 %, the difference was 12.60 % at the fourth point. As expected, the maximum displacement values were obtained at the peak point. Time-varying displacement values were obtained from two different analyses, which were consistent with each other. In addition, these values represent the effects of the wave motion on the structure. Changes in the motion of the structure owing to wave motion are also shown.

Figure 9 shows that damage affects the modal behaviour when compared to Cases I and III–VI, including the different damage situations of the same model over the natural frequency. The reduction in the modulus of elasticity also decreased the natural frequency from Case III to Case VI. However, this situation did

not cause any change in modal behaviour. When the mode shapes were examined, it was observed that the first modes were the torsion modes. In Case VII, where the damage type changed, the natural frequency value continued to decrease, whereas the same modal behaviour was observed for the other damage types. Considering that Case VII had three legs compared to Case II, the rupture of the leg had a negative effect on the natural frequency value, causing a 17.35 % decrease.

When the cases were examined according to the von Mises stress values, it was observed that the maximum stress occurred in Case II. In this case, the stress values differed between the feet, as shown in Figure 10. The stress was concentrated in the third leg. Sudden damage to the legs can be devastating. Although not as distinct as in Case II, a difference was observed in the stress values of the feet in Case VII. As expected, the lowest stress value occurred in the fourth ruptured leg. However, the difference between the stress distributions of the legs decreased in Case VI and seemed to show a homogeneous distribution compared to Case VII. In Case V, where the modulus of elasticity of the damaged leg was reduced by 20 %, the stress distribution in the feet became homogeneous. In addition, the stress distribution in the feet was homogeneous in Cases I, III, and IV. Among the damaged models, the most critical situation was observed in Case VII owing to the total stress value in all four legs and the difference in stress values between the legs. The stress distributions of the cases are shown in Figure 14.

When the cases were investigated according to the displacement values, as shown in Figure 10, there was an equal distribution between the feet in Case II, unlike the stress values. The maximum stress was obtained in this case. Although the displacement value in Case VII was smaller than that in Case II, the displacement values differed between the feet. As expected, a decrease in the displacement value was observed in the other cases, and the displacement values between the legs approached each other. Figure 13 shows the stress distributions for each case. The displacement and stress values in each leg are shown in Figure 10, and the variation in the reaction forces with the displacement in the feet where the maximum displacement occurs is shown in Figure 11. Minimal reaction force occurred in the ruptured leg of Case VII compared with the other four-legged models. By contrast, the maximum reaction force was obtained against the maximum displacement in Case II.

As can be seen from the displacement values that changed over time in Figure 12, damage to the leg changed the form of the displacement. The displacement in Cases I and II, including the undamaged situations, was similar to the wave motion, as shown in Figure 7, and the values remained constant in the band. As the modulus of elasticity was reduced in Cases III-VI, damping behaviour was observed in the displacement. As the damage ratio increases, the displacement frequency decreases. Therefore, the analysis time of Case III, shown in Figure 12, was maintained longer than that of the other cases, and displacement damping was observed. However, the displacement was not damped in Case 7, unlike the other damage types.

In this study, the flow environment surrounding the structure and structural results were also obtained. The structural displacements that change because of the movement and free-surface elevations of the wave at different time steps are shown in Figure 15. Using the free water surface model, the effect of wave motion on the unfluctuating water level on the structure was also considered. If the CEL technique had not been used, the movement above the non-fluctuating water level would have been ignored.

This study showed that the most critical results occurred in Case II due to the limited number of legs, as expected. In addition, the effect of different damage situations that may occur in one leg of the four-legged model on the structural behaviour was revealed both numerically and visually. Revealing the damping effect caused by the decrease in the elasticity modulus on the displacement of the structure, as well as the changes in the stress, natural frequency, and model behaviour, may also be added to the limitations of this study. Presenting these inferences both proportionally and visually will benefit future researchers studying similar subjects. A comparison of the two types of damage that may occur in a single region is also included. In addition to different damage models, such as pitting and wall thickness reduction, cases of damage to more than one region will be discussed in future studies. Furthermore, to examine the environmental effects in detail, wave theories and the effect of changes in wave arrival directions on damaged structures are also considered subjects for future studies.

REFERENCES

[1]   Zhang, P., Li, J., Gan, Y., Zhang, J., Qi X., Le, C., Ding, H.: Bearing capacity and load transfer of brace topological in offshore wind turbine jacket structure, Ocean Engineering, 199 (2020), doi: 10.1016/j.oceaneng.2020.107037.

[2]   Xie, Y., Huang, J., Li, X., Tian, X., Liu, G., Leng, D.: Experimental study on hydrodynamic characteristics of three truss-type legs of jack-up offshore platform, Ocean Engineering, 234 (2021). doi: 10.1016/j.oceaneng.2021.109305.

[3]   Zhu, B., Sun, C., Jahangiri, V.: Characterizing and mitigating ice-induced vibration of monopile offshore wind turbines, Ocean Engineering, 219 (2021). doi: 10.1016/j.oceaneng.2020.108406.

[4]   Dehghania, A., Aslani, F.: A review on defects in steel offshore structures and developed strengthening techniques, Structures, 20 (2019), pp. 635–657. doi: 10.1016/j.istruc.2019.06.002.

[5]   Asgarian, B., Shokrgozar, H.R.: A new bracing system for improvement of seismic performance of steel jacket type offshore platforms with float-over dec, Petroleum Science, 10 (2013), pp. 373–384. doi: 10.1007/s12182-013-0285-2.

[6]   Bao, X., Fan, T., Shi C., Yang, G.: One-dimensional convolutional neural network for damage detection of jacket-type offshore platforms, Ocean Engineering 219 (2021). doi: 10.1016/j.oceaneng.2020.108293.

[7]   Wang, S.: Damage detection in offshore platform structures from limited modal data, Applied Ocean Research, 41 (2013), pp. 48–56. doi: 10.1016/j.apor.2013.02.004.

[8]   Wang, S., Zhang, M., Li, H.: Damage localization of an offshore platform considering temperature variations, Mathematical Problems in Engineering, (2015), p. 954926. doi: 10.1155/2015/954926.

[9]   Gücüyen, E., Erdem, R.T.: Corrosion effects on structural behavior of jacket type offshore structures, Građevinar, 66 (2014) 11, pp. 981-986. doi: 10.14256/JCE.11262014.

[10] Gücüyen, E.: Numerical analysis of deteriorated sub-sea pipelines under environmental loads, Chinese Journal Of Mechanical Engineering, 28 (2015) 6, pp. 1163-1170. doi: 10.3901/CJME.2015.0909.111.

[11] Mazaheri, P., Asgarian, B., Gholami, H.: Assessment of strengthening, modification, and repair techniques for aging fixed offshore steel platforms, Applied Ocean Research, 110 (2021), 102612. doi: 10.1016/j.apor.2021.102612.

[12] Mujeeb-Ahmed, M.P., Ince, S.T., Paik, J.K.: Computational models for the structural crashworthiness analysis of a fixed-type offshore platform in collisions with an offshore supply vessel, Thin–Walled Structures, 154 (2020), 106868. doi: 10.1016/j.tws.2020.106868.

[13] Martínez, E.L., Quiroga, A.G., Jardini, A.L., Filho, R.M.: Computational fluid dynamics simulation of the water – sugar cane bagasse suspension in pipe with internal static mixer, Computer Aided Chemical Engineering, 26 (2009), pp. 683-688. doi: 10.1016/S1570-7946(09)70114-2.

[14] Leder, T. D., Leder, N., Hećimović, Z.: Split Metropolitan area surface temperature assessment with remote sensing method, Gradevinar, 68 (2016) 11, pp. 895-905. doi: 10.14256/JCE.1661.2016.

[15] Gücüyen, E., Erdem, R.T., Gökkuş, Ü.: FSI analysis of submarine outfall, Brodogradnja/Shipbilding, 67 (2016) 2, pp. 67-80. doi: 10.21278/brod67205.

[16] Korobenko, A., Yan, J., Gohari, S.M.I., Sarkar, S., Bazilevs, Y.: FSI Simulation of two back-to-back wind turbines in atmospheric boundary layer flow, Computers and Fluids, 158 (2017), pp. 167-175. doi: 10.1016/j.compfluid.2017.05.010.

[17] Liu, J.: A second-order changing-connectivity ALE scheme and its application to FSI with large convection of fluids and near contact of structures, Journal of Computational Physics, 304 (2016), pp. 380–423. doi: 10.1016/j.jcp.2015.10.015.

[18] Gücüyen, E., Yiğit, M.E., Erdem, R.T., Gökkuş, Ü.: Comparative analysis of tripod offshore structure, Gradevinar, 72 (2020) 11, pp. 1021-1030. doi: 10.14256/JCE.2848.2019.

[19] ABAQUS User's Manual, Version 6.12, SIMULIA, Dassault Systèmes Simulia Corp., 2015.

[20] Jalbi, S., Nikitas, G., Bhattacharya, S., Alexander, N.: Dynamic design considerations for offshore wind turbine jackets supported on multiple foundations, Marine Structures, 67 (2019), 102631. doi: 10.1016/j.marstruc.2019.05.009.

[21] Chakrabarti, S.: Handbook of Offshore Engineering, Elsevier Ltd, Illinois, USA, 2005.

[22] Dyrbye, C., Hansen, S.O.: Wind loads on structures, John Wiley & Sons, Ltd. United Kingdom, 2004.

[23] Barltrop, N.D.P., Adams, A.J.: Dynamics of Fixed Marine Structures, 3rd edition, Atkins Oil and Gas Engineering Limited, 1991.